RSC Advances

PAPER

View Article Online
View Journal | View Issue

Cite this: *RSC Adv.*, 2024, **14**, 22408

σ-Hole, lone-pair-hole, and π-hole site-based interactions in aerogen-comprising complexes: a comparative study†

Mahmoud A. A. Ibrahim, *[ab] Hassan A. A. Abuelliel,[a] Nayra A. M. Moussa, [ac] Al-shimaa S. M. Rady,[a] Shaban R. M. Sayed,[d] Mohamed A. El-Tayeb,[d] Muhammad Naeem Ahmed, [e] Mohamed Khaled Abd El-Rahman[f] and Tamer Shoeib *[g]

Herein, the potential of ZO_3 and ZF_2 aerogen-comprising molecules (where Z = Ar, Kr, and Xe) to engage in σ-, lp-, and π-hole site-based interactions was comparatively studied using various *ab initio* computations. For the first time, a premier in-depth elucidation of the external electric field (EEF) influence on the strength of the σ-, lp-, and π-hole site-based interactions within the $ZO_3/ZF_2\cdots NH_3$ and ⋯NCH complexes was addressed using oriented EEF with disparate magnitude. Upon the energetic features, σ-hole site-based interactions were noticed with the most prominent preferability in comparison to lp- and π-hole analogs. This finding was ensured by the negative interaction energy values of −11.65, −3.50, and −2.74 kcal mol^{-1} in the case of σ-, lp-, and π-hole site-based interactions within the $XeO_3\cdots$ and $XeF_2\cdots NH_3$ complexes, respectively. Detailedly, the strength of the σ- and lp-hole site-based interactions directly correlated with the atomic size of the aerogen atoms and the magnitude of the positively oriented EEF. Unexpectedly, an irregular correlation was noticed for the interaction energies of the π-hole site-based interactions with the size of the π-hole. Interestingly, the π-hole site-based interactions within Kr-comprising complexes exhibited higher negative interaction energies than the Ar- and Xe-comprising counterparts. Notwithstanding, a direct proportion between the interaction energies of the π-hole site-based interactions and π-hole size was obtained by employing EEF along the positive orientation with high strength. The present outcomes would be a fundamental basis for forthcoming progress in studying the σ-, lp-, and π-hole site-based interactions within aerogen-comprising complexes and their pertinent applications in materials science and crystal engineering.

Received 16th May 2024
Accepted 29th June 2024

DOI: 10.1039/d4ra03614j

rsc.li/rsc-advances

1. Introduction

Noncovalent interactions are indispensable in scientific research, enabling a deeper understanding of molecular behavior,[1,2] biomolecular processes,[3–5] and the design of advanced materials.[6,7] The extensive study of these interactions has provided valuable insights into their fundamental nature and essential features, contributing to advancements in multiple scientific fields. Among noncovalent interactions, hole interactions have gathered impressive interest due to their superior contributions in various fields including anion recognition,[8] ligand–acceptor interactions,[9,10] materials science,[11–13] drug discovery,[14,15] and supramolecular chemistry.[16–18]

In the literature, hole interactions can be categorized into several types, namely, σ-hole,[19] π-hole,[20] lone-pair (lp)-hole,[21] and radical ($R^{\bullet}$)-hole.[22] In detail, the concept of σ-hole was initially introduced to describe a region of positive or less negative electrostatic potential that extended along the σ-bond of covalently bonded elements. Subsequent research expanded this concept to include π-hole interactions, which involve the interactions between the Lewis bases and the positive electrostatic potential regions located almost perpendicular to the molecular entity of the chemical system. In parallel, extensive studies were conducted on the interactions of the Lewis bases

[a]*Computational Chemistry Laboratory, Chemistry Department, Faculty of Science, Minia University, Minia 61519, Egypt. E-mail: m.ibrahim@compchem.net*
[b]*School of Health Sciences, University of KwaZulu-Natal, Westville Campus, Durban 4000, South Africa*
[c]*Basic and Clinical Medical Science Department, Faculty of Dentistry, Deraya University, New Minya 61768, Egypt*
[d]*Department of Botany and Microbiology, College of Science, King Saud University, P.O. Box 2455, Riyadh 11451, Saudi Arabia*
[e]*Department of Chemistry, The University of Azad Jammu and Kashmir, Muzaffarabad 13100, Pakistan*
[f]*Department of Chemistry and Chemical Biology, Harvard University, 12 Oxford Street, Cambridge, MA 02138, USA*
[g]*Department of Chemistry, The American University in Cairo, New Cairo 11835, Egypt. E-mail: t.shoeib@aucegypt.edu*

† Electronic supplementary information (ESI) available. See DOI: https://doi.org/10.1039/d4ra03614j

with the positive molecular electrostatic potential of lp- and R˙-holes, which refers to electron-deficient regions located nearly opposite to the lp and R˙, respectively. These categories of interactions were basically labelled based on the element involved in the bond donation, corresponding to its placement in the periodic table, as triel (Group III),[23–25] tetrel (Group IV),[26–29] pnicogen (Group V),[30–33] chalcogen (Group VI),[34,35] halogen (Group VII),[19,35–38] and aerogen (Group VIII)[39–41] bonds.

In recent years, immense theoretical and experimental studies have been performed to thoroughly unveil the features of aerogen (*i.e.*, noble gas)-comprising complexes. Upon exploring the Inorganic Crystal Structure Database (ICSD), Gomila and Frontera documented the existence of interactions of xenon fluorides with several electron donors.[42] Carvalho *et al.* adequately ensured the occurrence of aerogen bonds in the gas phase with disparate favorability that proportionally correlated with the atomic size of the interacted aerogen atom.[43]

Noble gas oxides are deemed one of the most common aerogen bond donors that were employed to divulge the aerogen interactions. Accordingly, their geometries and spectral characteristics were thoroughly investigated.[44–47] In a landmark study, Esrafili *et al.* reported the effect of the substituent on the strength of the aerogen bond interactions of ZO_3 (Z = Kr and Xe) with different nitrogen bases using a wide range of quantum mechanical calculations.[41] It was declared that the low reactive ArO_3, KrO_3, XeO_3, and XeF_2O molecules exhibited preferential potentiality to interact with various electron donors (NH_3, CH_3CN, Cl^-, and Br^-) with interaction energies of up to -37.2 kcal mol^{-1}.[39]

According to the literature, various types of holes could coexist within individual molecular entities, appearing throughout the molecular structure either on the same atom or in different atoms. While previous studies have reported the presence of multiple holes on different atoms within the same molecular entity,[48–53] researchers have recently focused their investigations on characterizing the specific attributes of various hole interactions occurring on a single atom. In this context, the σ-hole and π-hole interactions in the case of KrF_2O and XeF_2O molecules have been extensively studied and outlined the electrostatic term as the most predominant contributor to the total interaction energies of their corresponding complexes.[46,54] On the other hand, in molecules such as NF_3/PF_3 (ref. 55) and XeO_3,[47] researchers comparatively examined the σ- and lp-hole site-based interactions occurring on the same atom, demonstrating the higher preference for σ-hole interactions when interacting with Lewis bases, as compared to other types of holes.

For the first time, this investigation would unveil the potentiality of aerogen-comprising molecules to engage in σ-, lp- and π-hole site-based interactions with Lewis bases (LB) within the $ZO_3\cdots$ and $ZF_2\cdots$LB complexes, respectively, as illustrated in Fig. 1. To pursue the research purpose, sundry quantum computations involving geometry optimization, point of charge (PoC) approach, electrostatic potential (ESP) analysis, and interaction energy were herein executed. To elucidate the physical force that dominates the interactions under investigation, the symmetry-adapted perturbation theory (SAPT) analysis was performed. Topological features of the studied interactions were also unveiled in the context of the quantum theory of atoms in molecules (QTAIM) and noncovalent interaction (NCI) index analyses. A premier insight into the oriented external electric field (EEF) influence on the strength of the σ-, lp-, and π-hole site-based interactions was announced (Fig. 1). The emerging findings would be a substantial base for the forthcoming studies relevant to σ-, lp-, and π-hole site-based interactions and their utilization in materials science and crystal engineering research.

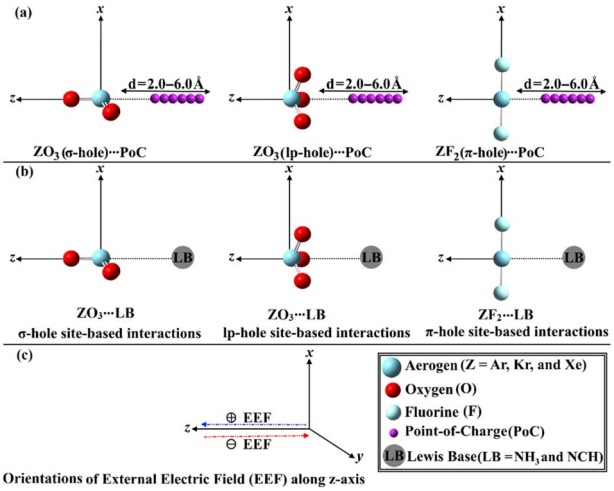

Fig. 1 Representative graph of (a) $ZO_3\cdots/ZF_2\cdots$PoC systems, (b) $ZO_3\cdots/ZF_2\cdots$LB complexes, and (c) orientations of the employed EEF. Positive (+) and negative (−) signs refer to the orientation of the EEF along the *z*-axis of the studied aerogen-comprising molecules and their corresponding complexes.

2. Results and discussion

2.1. ESP analysis

ESP analysis was herein executed on the optimized monomers to unveil the nature of the chemical systems, either nucleophilic

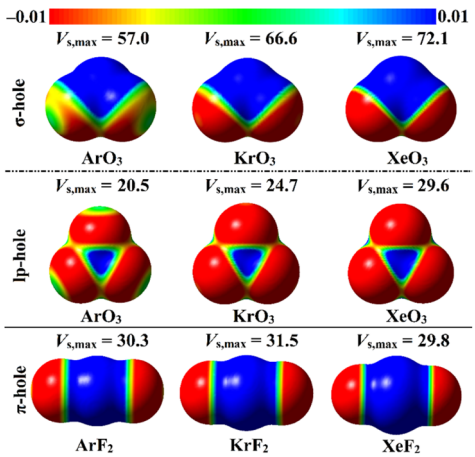

Fig. 2 MEP maps of the optimized ZO_3 and ZF_2 monomers (where Z = Ar, Kr, and Xe) graphed utilizing 0.002 au electron density contours. $V_{s,max}$ values are in kcal mol^{-1}.

or electrophilic, by generating MEP maps and assessing the $V_{s,max}$ values. MEP maps and the $V_{s,max}$ values are shown in Fig. 2.

Inspecting Fig. 2, σ-/lp- and π-holes were obviously noticed over the molecular entities of the studied ZO_3 and ZF_2 monomers, respectively. Apparently, the most prominent blue positive region over the surface of the aerogen-comprising molecules was ascribed to the σ-hole that also showed the largest $V_{s,max}$ values. As a numerical illustration, the $V_{s,max}$ surrounding the Xe's σ-, lp-, and π-holes were 72.1, 29.6, and 29.8 kcal mol^{-1}, respectively.

Concerning the ZO_3 molecules, a proportional correlation was noticed for the size and magnitude of the σ- and lp-holes with the aerogen-atomic size. For instance, the σ-hole of the aerogen atom in the ArO_3, KrO_3, and XeO_3 molecules showed $V_{s,max}$ quantities of 57.0, 66.6, and 72.1 kcal mol^{-1}, respectively. This trend was also confirmed in the literature.[56] While the π-hole of the ZF_2 monomers enlarged according to the successive XeF_2 < ArF_2 < KrF_2 pattern. This finding reflected the irregular correlation of the π-hole size and magnitude with the aerogen atomic size. As quantitative evidence, the aerogen π-hole in the ArF_2, KrF_2, and XeF_2 molecules exhibited $V_{s,max}$ with values of 30.3, 31.5, and 29.8 kcal mol^{-1}, respectively.

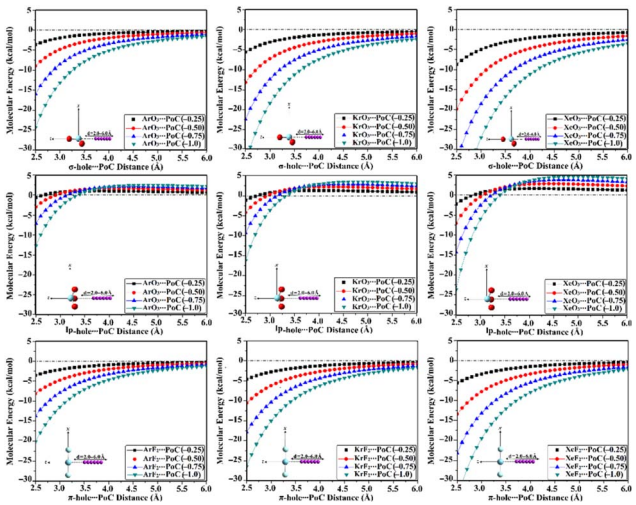

Fig. 3 Curves of molecular energy (in kcal mol^{-1}) of $ZO_3\cdots$ and $ZF_2\cdots$ PoC systems (where Z = Ar, Kr, and Xe) at the σ-/lp- and π-hole$\cdots$PoC distances ranging from 2.5 to 6.0 Å.

2.2. PoC calculations

The PoC methodology, a recently announced approach, is established as an efficient way for conducting a comprehensive analysis of noncovalent interactions from an electrostatic standpoint.[57] In accordance with this approach, negative PoCs with values of −0.25, −0.50, −0.75, and −1.0 au were adopted to simulate the effect of Lewis basicity on the examined interactions. The evaluation of the $E_{stabilization}$ of the $ZO_3\cdots$ and $ZF_2\cdots$ PoC systems was conducted by examining the Z$\cdots$PoC distances within the scope of 2.5–6.0 Å (Fig. 3). $E_{stabilization}$ of the $ZO_3\cdots$ and $ZF_2\cdots$PoC systems at the σ-, lp-, and π-hole$\cdots$PoC distances of 2.5 Å are shown in Table 1.

As illustrated in Fig. 3, the stabilization energy of the $ZO_3\cdots$ and $ZF_2\cdots$PoC systems boosted as the σ-/lp- and π-hole$\cdots$PoC intermolecular distance diminished, respectively. Apparently, destabilization energies were noticed in the case of the $ZO_3\cdots$ PoC systems at the most extended lp-hole$\cdots$PoC distances only. This exceptional case could be mainly ascribed to the lowest positive lp-holes of the aerogen bond donor and the role of the repulsive forces of the oxygen atoms with the negative PoC in the overall interactions. The obtained proportional and reverse correlations, in successive, of the destabilization and stabilization energies with the σ-/lp-/π-hole$\cdots$PoC intermolecular distances, announced the opulent effect of the Z$\cdots$PoC intermolecular distances on the aerogen$\cdots$Lewis base interactions.

The quantitative data listed in Table 1 unveiled that all the $ZO_3\cdots$ and $ZF_2\cdots$PoC systems showed towering $E_{stabilization}$ values at a distance of 2.5 Å, with the following order: π-hole < lp-hole < σ-hole. As a numerical illustration, $E_{stabilization}$ values of the Xe-comprising molecule$\cdots$PoC system at the σ-, lp-, and π-hole$\cdots$PoC distance of 2.5 Å were −8.78, −2.26, and −5.63 kcal mol^{-1}, respectively. Generally, the PoC energetic outcomes declared the synchronization of $E_{stabilization}$ with the aerogen atomic size. For instance, $ArO_3\cdots$, $KrO_3\cdots$, and $XeO_3\cdots$ PoC systems showed $E_{stabilization}$ of −3.65, −5.62, and

Table 1 $E_{stabilization}$ values (in kcal mol^{-1}) of the $ZO_3\cdots$ and $ZF_2\cdots$PoC systems (where Z = Ar, Kr, and Xe) at the σ-, lp-, and π-hole$\cdots$PoC distances of 2.5 Å

		$E_{stabilization}$			
Site	System	PoC = −0.25 au	PoC = −0.50 au	PoC = −0.75 au	PoC = −1.0 au
σ-Hole	$ArO_3\cdots$PoC	−3.65	−9.00	−15.92	−24.35
	$KrO_3\cdots$PoC	−5.62	−13.14	−22.42	−33.36
	$XeO_3\cdots$PoC	−8.78	−19.86	−33.07	−48.25
Lp-hole	$ArO_3\cdots$PoC	−0.59	−2.99	−7.08	−12.76
	$KrO_3\cdots$PoC	−1.06	−4.22	−9.31	−16.24
	$XeO_3\cdots$PoC	−2.26	−7.08	−14.29	−23.73
π-Hole	$ArF_2\cdots$PoC	−3.56	−8.14	−13.70	−20.21
	$KrF_2\cdots$PoC	−4.61	−10.60	−17.88	−26.38
	$XeF_2\cdots$PoC	−5.63	−13.40	−23.11	−34.61

−8.78 kcal mol^{-1}, respectively, employing −0.25 au PoC at the σ-hole···PoC distance of 2.5 Å. It is worth mentioning that evident amelioration of the $E_{stabilization}$ values was noticed by boosting the adopted PoC negativity (*i.e.*, Lewis basicity). Numerically, the XeO_3···PoC system at σ-hole···PoC of 2.5 Å exhibited $E_{stabilization}$ values of −8.78, −19.86, −33.07, and −48.25 kcal mol^{-1} using PoC with values of −0.25, −0.50, −0.75, and −1.0 au, respectively.

2.3. Interaction energy

In order to assess the propensity of aerogen-comprising molecules to establish σ-/lp- and π-hole site-based interactions, ZO_3··· and ZF_2···LB complexes were herein investigated in a detailed manner, respectively. Geometry optimization calculations were first executed for the scouted complexes (Fig. 4).

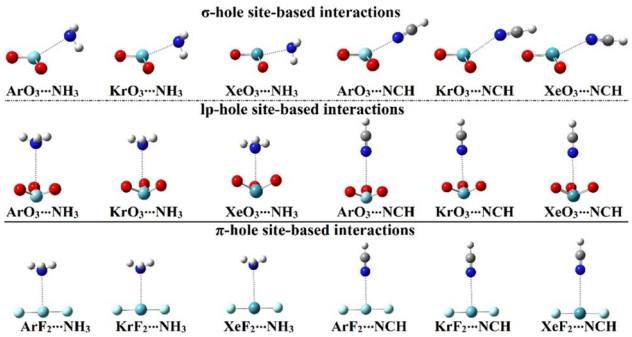

Fig. 4 Optimized structures of the σ-/lp- and π-hole site-based interactions within the ZO_3··· and ZF_2···LB complexes, respectively (where Z = Ar, Kr, and Xe; LB = NH_3 and NCH).

Interaction energies were calculated relying on the optimized geometries at the same level of theory and then benchmarked at the CCDS(T)/CBS level of theory (Table 2).

As evident in Fig. 4, the aerogen-comprising molecules under investigation potentially interacted with Lewis bases, forming σ-/lp- and π-hole site-based interactions within the ZO_3··· and ZF_2···LB complexes, respectively. The occurrence of the abovementioned interactions was confirmed by the resulting negative interaction energy values, as compiled in Table 2.

Concerning the σ- and lp-hole site-based interactions, towering negative interaction energy values were denoted for the ZO_3···LB complexes by boosting the aerogen atomic size, which is in line with the EP and PoC affirmations. For instance, the σ-/lp-hole site-based interaction showed $E_{MP2/aug\text{-}cc\text{-}pVTZ(PP)}$ values of −6.07/−0.58, −8.34/−1.30, and −10.92/−3.76 kcal mol^{-1} for the ArO_3···, KrO_3···, and XeO_3···NH_3 complexes, respectively. While the π-hole site-based interactions energetic quantities indicated that the Kr-comprising complexes exhibited higher negative values than their Ar- and Xe-comprising counterparts, indicating an irregular correlation with the size of the π-hole. For example, the π-hole site-based interactions within the ArF_2···, KrF_2···, and XeF_2···NH_3 complexes were observed with $E_{MP2/aug\text{-}cc\text{-}pVTZ(PP)}$ of −2.83, −3.23, and −3.03 kcal mol^{-1}, respectively.

Furthermore, the studied aerogen-comprising complexes were denoted with higher preferability in the case of NH_3-involved complexes in comparison to the NCH-based analogs. As a numerical evidence, the σ-hole site-based interactions within the XeO_3···NH_3 and ···NCH complexes had $E_{MP2/aug\text{-}cc\text{-}pVTZ(PP)}$ values of −11.65 and −7.67 kcal mol^{-1}, respectively.

Table 2 Complexation parameters and interaction energies given at the MP2/aug-cc-pVTZ(PP) ($E_{MP2/aug\text{-}cc\text{-}pVTZ(PP)}$) and CCSD(T)/CBS ($E_{CCSD(T)/CBS}$) levels of theory for the σ-/lp- and π-hole site-based interactions within the ZO_3··· and ZF_2···LB complexes, respectively (where Z = Ar, Kr, and Xe; LB = NH_3 and NCH)

		Complexation parameters		Interaction energy	
Site	Complex	D^a (Å)	θ^b (degree)	$E_{MP2/aug\text{-}cc\text{-}pVTZ(PP)}$ (kcal mol^{-1})	$E_{CCSD(T)/CBS}$ (kcal mol^{-1})
σ-Hole	ArO_3···NH_3	2.86	147.2	−6.56	−6.07
	KrO_3···NH_3	2.80	158.7	−8.87	−8.34
	XeO_3···NH_3	2.77	170.6	−11.65	−10.92
Lp-hole	ArO_3···NH_3	3.56	180.0	−0.30	−0.58
	KrO_3···NH_3	3.38	179.9	−0.92	−1.30
	XeO_3···NH_3	3.01	179.9	−3.50	−3.76
π-Hole	ArF_2···NH_3	3.17	90.4	−2.76	−2.83
	KrF_2···NH_3	3.27	90.3	−3.01	−3.23
	XeF_2···NH_3	3.48	90.3	−2.74	−3.03
σ-Hole	ArO_3···NCH	2.88	139.0	−5.10	−4.45
	KrO_3···NCH	2.88	150.3	−6.42	−5.76
	XeO_3···NCH	2.93	162.5	−7.67	−6.87
Lp-hole	ArO_3···NCH	3.52	179.9	−0.17	−0.24
	KrO_3···NCH	3.42	179.9	−0.36	−0.43
	XeO_3···NCH	3.30	179.8	−0.93	−0.96
π-Hole	ArF_2···NCH	3.12	90.4	−2.28	−2.15
	KrF_2···NCH	3.22	90.3	−2.48	−2.45
	XeF_2···NCH	3.44	90.4	−2.33	−2.36

[a] *D* refers to Z···N bond distance. [b] θ refers to ∠O/F-Z···N bond angle in the σ-/π-hole site-based interactions and ∠Z-center···N bond angle in the lp-hole site-based interactions.

Among the studied interactions, the highest negative interaction energy values were ascribed to the σ-hole site-based interactions, which was in line with the ESP affirmations. For example, the σ-/lp- and π-hole site-based interactions were found in the $XeO_3\cdots$ and $XeF_2\cdots NH_3$ complexes with MP2 energetic values of −11.65/–3.50 and −2.74 kcal mol^{-1} along with positive σ-/lp- and π-hole $V_{s,max}$ values of 72.1/29.6 and 29.8 kcal mol^{-1} for the XeO_3 and XeF_2 monomers, respectively. Moreover, a nearly similar pattern was detected between the $E_{MP2/aug\text{-}cc\text{-}pVTZ(PP)}$ and $E_{CCSD(T)/CBS}$ values, confirming the precision of the opted MP2/aug-cc-PVTZ level of theory in the executed computations.

2.4. SAPT analysis

To divulge the physical nature of the σ-/lp- and π-hole site-based interactions, SAPT analysis was performed on the optimized $ZO_3\cdots$ and $ZF_2\cdots$LB complexes, respectively. Table 3 compiles total SAPT2+(3)dMP2 energy and its principal physical energetic components. The energy differences (ΔΔE) between the $E_{MP2/aug\text{-}cc\text{-}pVTZ(PP)}$ and E_{SAPT} values were also evaluated and are listed in Table 3.

Based on the collected data in Table 3, negative values of E_{elst}, E_{disp} and E_{ind} components were observed, outlining their appreciable contributions to the σ-/lp- and π-hole site-based attractive interactions in all the considered $ZO_3\cdots$ and $ZF_2\cdots$LB complexes, respectively. Illustratively, the σ-hole site-based interaction within the $XeO_3\cdots NH_3$ complex had E_{elst}, E_{disp}, and E_{ind} values of −24.25, −3.93, and −1.49 kcal mol^{-1}, respectively. On the contrary, positive E_{exch} values unveiled the unpreferable impact of exchange forces on all the studied interactions.

SAPT findings generally demonstrated the substantial contributions of E_{elst} to all the considered interactions, with an exception for the weak lp-hole site-based interactions. For the latter exceptional interactions, the E_{disp} showed the highest dominance amplitude toward the attractive forces with values up to −3.96 in the case of the $XeO_3\cdots$NCH complex.

It is worth noting that the adopted SAPT calculations showed tiny ΔΔE values, ensuring the apparent accuracy of the utilized SAPT level of the theory. In general, the negative E_{elst}, E_{disp}, and E_{ind} values exhibited a proportional correlation with the interaction energy pattern. As numerical evidence, E_{elst} values of the σ-hole site-based interactions in the $XeO_3\cdots NH_3$ and ⋯NCH complexes were −24.25 and −11.14 kcal mol^{-1} along with MP2 energetic quantities of −11.65 and −7.67 kcal mol^{-1}, respectively.

2.5. QTAIM calculations

Using QTAIM theory, bond critical points (BCPs) and bond baths (BPs) were extracted and are shown in Fig. 5. Besides, Laplacian ($\nabla^2\rho_b$), total energy density (H_b), and electron density (ρ_b) were assessed and are gathered in Table 4.

According to the displayed data in Fig. 5, one BP and BCP were observed between the aerogen-comprising molecules and the NH_3 and NCH Lewis bases within the σ- and π-hole site-based interactions. This finding assured the potential of the ZO_3 and ZF_2 molecules to form σ- and π-hole site-based interactions, respectively. While three BPs and BCPs were noticed in the lp-hole site-based interactions of all studied complexes other than Xe-comprising complexes. This observation outlined the predominant contributions of the oxygen atoms to the interactions within Ar- and Kr-comprising complexes. The occurrence of sole BP within the Xe-comprising complexes unveils the domination of the attractive forces between the positive hole and the negative Lewis base.

From the recorded data in Table 4, small values of ρ_b and positive values of $\nabla^2\rho_b$ and H_b were denoted for almost all the inspected complexes, unveiling that the interactions

Table 3 E_{SAPT}, E_{elst}, E_{exch}, E_{ind}, E_{disp}, and ΔΔE of the σ-/lp- and π-hole site-based interactions within the $ZO_3\cdots$ and $ZF_2\cdots$LB complexes, respectively (where Z = Ar, Kr, and Xe; LB = NH_3 and NCH)

Site	Complex	E_{elst} (kcal mol^{-1})	E_{disp} (kcal mol^{-1})	E_{exch} (kcal mol^{-1})	E_{ind} (kcal mol^{-1})	E_{SAPT}[a] (kcal mol^{-1})	ΔΔE[b]
σ-Hole	$ArO_3\cdots NH_3$	−11.80	−3.93	10.35	−1.49	−6.86	−0.30
	$KrO_3\cdots NH_3$	−16.43	−5.46	16.59	−3.75	−9.05	−0.18
	$XeO_3\cdots NH_3$	−24.25	−7.61	27.88	−7.84	−11.82	−0.17
Lp-hole	$ArO_3\cdots NH_3$	−1.41	−2.29	3.38	−0.07	−0.39	−0.09
	$KrO_3\cdots NH_3$	−3.72	−3.51	6.33	−0.19	−1.10	−0.18
	$XeO_3\cdots NH_3$	−14.41	−7.08	19.91	−2.14	−3.72	−0.22
π-Hole	$ArF_2\cdots NH_3$	−4.50	−1.93	3.68	−0.21	−2.97	−0.21
	$KrF_2\cdots NH_3$	−4.79	−2.02	4.01	−0.44	−3.23	−0.22
	$XeF_2\cdots NH_3$	−4.46	−1.98	4.09	−0.55	−2.91	−0.17
σ-Hole	$ArO_3\cdots NCH$	−6.72	−3.05	5.49	−0.87	−5.15	−0.05
	$KrO_3\cdots NCH$	−8.69	−3.88	8.18	−1.90	−6.30	−0.02
	$XeO_3\cdots NCH$	−11.14	−4.89	11.8	−3.24	−7.47	0.20
Lp-hole	$ArO_3\cdots NCH$	−0.26	−2.02	2.19	−0.02	−0.11	−0.04
	$KrO_3\cdots NCH$	−0.95	−2.76	3.45	−0.06	−0.32	−0.3
	$XeO_3\cdots NCH$	−2.78	−3.96	6.15	−0.27	−0.88	0.05
π-Hole	$ArF_2\cdots NCH$	−2.81	−1.74	2.32	−0.09	−2.32	−0.04
	$KrF_2\cdots NCH$	−3.15	−1.83	2.74	−0.27	−2.50	−0.3
	$XeF_2\cdots NCH$	−3.06	−1.80	2.92	−0.37	−2.31	0.02

[a] $E_{SAPT} = E_{elst} + E_{exch} + E_{disp} + E_{ind}$. [b] $\Delta\Delta E = E_{MP2/aug\text{-}cc\text{-}pVTZ(PP)} - E_{SAPT}$.

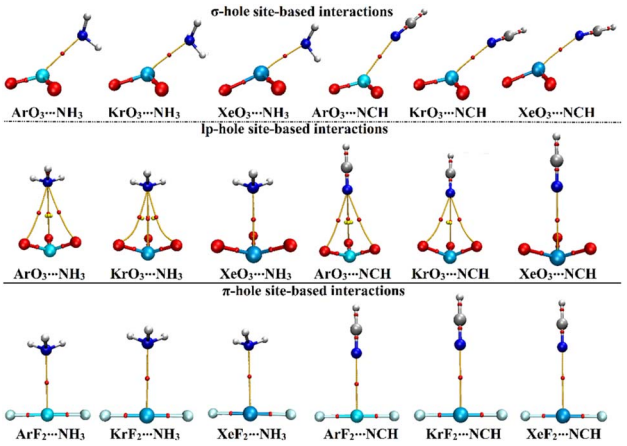

Fig. 5 QTAIM plots of the σ-/lp- and π-hole site-based interactions within the $ZO_3\cdots$ and $ZF_2\cdots$LB complexes, respectively (where Z = Ar, Kr, and Xe; LB = NH_3 and NCH).

Table 4 ρ_b, $\nabla^2\rho_b$, and H_b at BCPs of the σ-/lp- and π-hole site-based interactions within the $ZO_3\cdots$ and $ZF_2\cdots$LB complexes, respectively (where Z = Ar, Kr, and Xe; LB = NH_3 and NCH)

Site	Complex	ρ_b (au)	$\nabla^2\rho_b$ (au)	H_b (au)
σ-Hole	$ArO_3\cdots NH_3$	0.01729	0.06579	0.00197
	$KrO_3\cdots NH_3$	0.02361	0.07577	0.00087
	$XeO_3\cdots NH_3$	0.03166	0.08007	−0.00147
Lp-hole	$ArO_3\cdots NH_3$	0.00495	0.01580	0.00072
	$KrO_3\cdots NH_3$	0.00741	0.02900	0.00124
	$XeO_3\cdots NH_3$	0.01909	0.05595	0.00081
π-Hole	$ArF_2\cdots NH_3$	0.00916	0.03510	0.00186
	$KrF_2\cdots NH_3$	0.00985	0.03306	0.00142
	$XeF_2\cdots NH_3$	0.00918	0.02687	0.00108
σ-Hole	$ArO_3\cdots NCH$	0.01438	0.06288	0.00262
	$KrO_3\cdots NCH$	0.01747	0.06696	0.00201
	$XeO_3\cdots NCH$	0.02015	0.06727	0.00146
Lp-hole	$ArO_3\cdots NCH$	0.00442	0.01598	0.00085
	$KrO_3\cdots NCH$	0.00579	0.02181	0.00110
	$XeO_3\cdots NCH$	0.00886	0.03520	0.00165
π-Hole	$ArF_2\cdots NCH$	0.00845	0.03784	0.00228
	$KrF_2\cdots NCH$	0.00906	0.03563	0.00183
	$XeF_2\cdots NCH$	0.00834	0.02883	0.00144

understudy have a closed-shell nature except for the σ-hole site-based interaction within the $XeO_3\cdots NH_3$ complex. The latter interaction was detected by a negative H_b value, outlining its partially covalent nature. In general, the ρ_b, $\nabla^2\rho_b$, and H_b trends directly correlated with the interaction energy trend. For instance, the σ-hole site-based interactions of the $ArO_3\cdots$, $KrO_3\cdots$, and $XeO_3\cdots NH_3$ complexes had ρ_b with values of 0.01729, 0.02361, and 0.22483 au accompanied by $E_{MP2/aug\text{-}cc\text{-}pVTZ(PP)}$ values of −6.07, −8.34, and −10.92, kcal mol^{-1}, respectively.

2.6. NCI calculations

NCI index analysis unveils either the attractive or repulsive forces of the noncovalent interactions between the chemical species.[58,59] In this regard, NCI plots were generated using a 0.50 au reduced density gradient with a colored scale ranging from

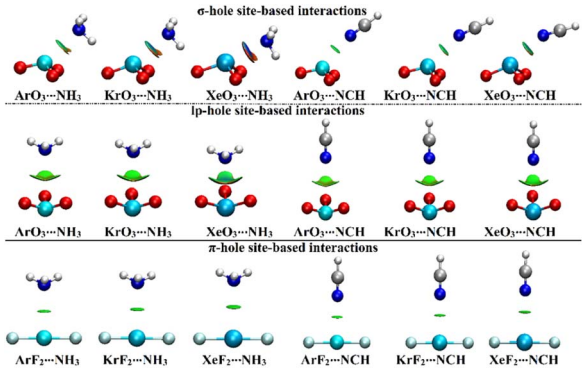

Fig. 6 NCI plots of the σ-/lp- and π-hole site-based interactions within the $ZO_3\cdots$ and $ZF_2\cdots$LB complexes, respectively (where Z = Ar, Kr, and Xe; LB = NH_3 and NCH).

blue ($\mathrm{sign}(\lambda_2)\rho = -0.035$ au) to red ($\mathrm{sign}(\lambda_2)\rho = +0.020$ au) and are displayed in Fig. 6.

As delineated in Fig. 6, the occurrence of the σ-/lp- and π-hole site-based interactions within the $ZO_3\cdots$ and $ZF_2\cdots$LB complexes, respectively, was affirmed by the existence of the green isosurfaces between the interacted species. Conspicuously, blue-colored isosurfaces were found in the σ-hole site-based interactions of the Xe-comprising complexes, reflecting their partially covalent nature. For lp-hole site-based interactions, NCI plots were in line with the affirmations of the QTAIM, which demonstrated the contributions of the substituents to the interactions within all the considered complexes.

2.7. EEF effect

EEF was earlier reported to have an immense effect on the nature and strength of noncovalent interactions.[60–62] In this regard, the EEF effect on the σ-, lp-, and π-hole site-based

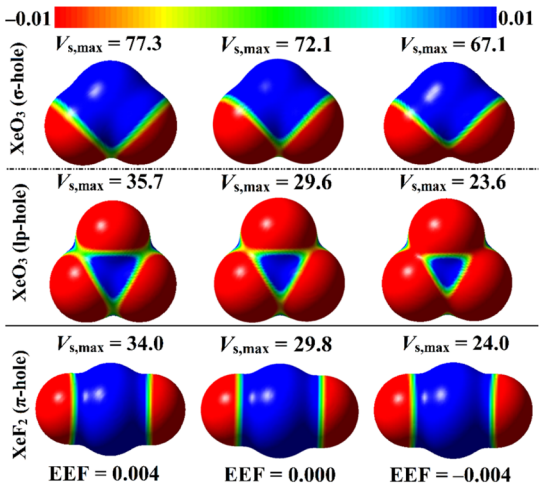

Fig. 7 MEP maps of the optimized XeO_3 and XeF_2 monomers under the +0.004, 0.000 and −0.004 au EEF conditions. $V_{s,max}$ values at the σ-/lp- and π-hole sites of the XeO_3 and XeF_2 monomers, respectively, are in kcal mol^{-1}.

interactions was thoroughly assessed (Fig. 1). The geometrical optimization and MEP computations were initially performed for the aerogen-comprising molecules employing ±0.004, ±0.008, and ±0.016 au EEF (Fig. S1–S3†). Fig. 7 shows the visualized MEP maps of the optimized Xe-comprising molecules in the presence of ±0.004 au EEF.

According to Fig. 7, applying a positively oriented EEF increased the σ-, lp-, and π-hole size on the examined molecules, whereas using a negatively oriented EEF lowered it. For example, the σ-hole magnitudes of the XeO_3 molecule were noticed with $V_{s,max}$ values of 77.3, 67.1, and 72.1 kcal mol^{-1} in the presence of +0.004, −0.004, and 0.000 au EEF, respectively. Based on the displayed data in Fig. S1–S3,† the preferable contribution of the EEF was obviously denoted by boosting the magnitude of the positively oriented EEF. Numerically, the $V_{s,max}$ values of the σ-hole of the XeO_3 molecule were 77.3, 82.6, and 93.5 kcal mol^{-1} under the effect of 0.004, 0.008, and 0.016 au EEF, respectively. Therefore, the subsequent analyses of the examined interactions were conducted solely under the conditions of the positively oriented EEF.

Under the positively oriented EEF influence, geometrical optimization calculations were executed using variant EEF magnitudes ranging from 0.004 to 0.016 au for the complexes under study. Based on the optimized geometries of the investigated complexes, the interaction energy computations were performed using +0.004, +0.008, and +0.016 au EEF (Table 5).

As summarized in Table 5, negative interaction energy values of the examined complexes increased as the strength of the positively oriented EEF expanded. Illustratively, interaction energy values of −13.78, −15.98, and −22.07 kcal mol^{-1} were observed for the σ-hole site-based interaction within the $XeO_3\cdots NH_3$ complexes by utilizing +0.004, +0.008, and +0.016 au EEF, respectively.

Concerning π-hole site-based interactions, there was a remarkable direct correlation between the aerogen atomic size and the preferability of the interactions under investigation, particularly under the influence of the positively oriented EEF with the highest magnitude (*i.e.*, 0.016 au EEF). For instance, the π-hole site-based interactions within $ArF_2\cdots$, $KrF_2\cdots$, and $XeF_2\cdots NH_3$ complexes in the presence of EEF with a magnitude of 0.016 au showed interaction energy of −4.46, −5.17, and −5.46 kcal mol^{-1}, respectively. In comparison, the π-hole site-based interactions within the $ArF_2\cdots$, $KrF_2\cdots$, and $XeF_2\cdots NH_3$ complexes in the absence of the EEF had interaction energy values of −2.83, −3.23, and −3.03 kcal mol^{-1}, respectively (Table 2). Such observations confirmed the predominant role of the EEF in controlling the interactions under investigation.

Table 5 Complexation parameters and interaction energies of the σ-/lp- and π-hole site-based interactions within the $ZO_3\cdots$ and $ZF_2\cdots$LB complexes (where Z = Ar, Kr, and Xe; LB = NH_3 and NCH) under the conditions of the positively oriented EEF with disparate strengths in the range of 0.004–0016 au

			$ZO_3/ZF_2\cdots NH_3$			$ZO_3/ZF_2\cdots NCH$		
Complexes		EEF (au)	D^a (Å)	θ^b (degree)	E (kcal mol^{-1})	D^a (Å)	θ^b (degree)	E (kcal mol^{-1})
σ-Hole	$ArO_3\cdots$LB	0.004	2.83	150.1	−7.23	2.85	146.2	−5.69
		0.008	2.81	152.1	−7.94	2.82	148.8	−6.39
		0.016	2.75	155.8	−9.72	2.77	152.7	−8.12
	$KrO_3\cdots$LB	0.004	2.76	160.3	−10.08	2.84	153.8	−7.36
		0.008	2.73	161.6	−11.40	2.81	155.8	−8.45
		0.016	2.62	165.3	−14.93	2.73	159.1	−11.12
	$XeO_3\cdots$LB	0.004	2.73	171.9	−13.78	2.88	163.7	−9.05
		0.008	2.66	173.4	−15.98	2.84	165.1	−10.67
		0.016	2.56	176.4	−22.07	2.73	168.4	−14.78
Lp-hole	$ArO_3\cdots$LB	0.004	3.51	179.9	−0.57	3.47	179.9	−0.42
		0.008	3.47	179.9	−0.89	3.42	179.8	−0.72
		0.016	3.39	179.9	−1.65	3.34	179.9	−1.48
	$KrO_3\cdots$LB	0.004	3.31	179.1	−1.47	3.36	179.9	−0.76
		0.008	3.24	179.6	−2.05	3.30	179.9	−1.24
		0.016	3.10	179.7	−3.71	3.19	180.0	−2.48
	$XeO_3\cdots$LB	0.004	2.78	179.9	−6.81	3.21	179.9	−1.73
		0.008	2.49	179.8	−14.17	3.11	179.9	−2.77
		0.016	2.34	179.7	−26.85	2.90	179.9	−5.99
π-Hole	$ArF_2\cdots$LB	0.004	3.16	179.6	−3.14	3.10	179.9	−2.67
		0.008	3.14	91.9	−3.55	3.08	91.8	−3.11
		0.016	3.12	93.1	−4.46	3.04	93.2	−4.10
	$KrF_2\cdots$LB	0.004	3.25	90.8	−3.49	3.20	90.9	−2.96
		0.008	3.23	91.5	−4.01	3.17	91.6	−3.50
		0.016	3.18	92.9	−5.17	3.11	93.0	−4.74
	$XeF_2\cdots$LB	0.004	3.44	90.7	−3.32	3.40	91.6	−2.90
		0.008	3.41	91.6	−3.97	3.36	92.5	−3.56
		0.016	3.35	93.3	−5.46	3.28	94.2	−5.12

[a] D refers to Z⋯N bond distance. [b] θ refers to the ∠O/F-Z⋯N bond angle in the σ-/π-hole site-based interactions and ∠Z-center⋯N bond angle in the lp-hole site-based interactions.

3. Computational methods

The potentiality of ZO_3 and ZF_2 aerogen-comprising molecules to form σ-/lp- and π-hole site-based interactions, respectively, was herein unveiled using NH_3 and NCH Lewis bases. In this regard, all the adopted monomers and complexes were first subjected to geometry optimization using the MP2 method[63] accompanied by the aug-cc-pVTZ basis set[64,65] for all the employed atoms except Kr and Xe. The relativistic effects of the latter atoms were considered by incorporating the pseudopotentials (PP).[65,66]

On the optimized monomers, ESP analysis was performed to demonstrate the nucleophilic and electrophilic nature of the systems under investigation. Subsequently, molecular electrostatic potential (MEP) maps were graphed by employing 0.002 au electron density envelopes in accordance with the literature suggestions.[67] As well, the maximum positive electrostatic potential ($V_{s,max}$) values were assessed with the aid of Multiwfn 3.7 software.[68]

The PoC method was invoked as a dependable tool for studying the potentiality of the chemical systems to engage in σ-,[57,69] lp-,[55] and π-hole[70] site-based interactions from an electrostatic perspective. Using PoC terminology, the influence of Lewis basicity on the stabilization energy ($E_{stabilization}$) of the $ZO_3\cdots$ and $ZF_2\cdots$PoC systems was divulged using −0.25, −0.50, −0.75, and −1.0 au, as demonstrated in eqn (1). Detailedly, the ZO_3 and ZF_2 monomers were subjected to negative PoC *via* three distinct interaction sites, namely the σ-, lp-, and π-hole sites (see Fig. 1). The σ-, lp-, and π-hole$\cdots$PoC distances were set using a range starting from 2.5 Å to 6.0 Å with a step size of 0.1 Å.

$$E_{stabilization} = E_{aerogen\text{-}comprising\ molecule\cdots PoC} - E_{aerogen\text{-}comprising\ molecule} \quad (1)$$

On the optimized structures of the investigated complexes, interaction energies were computed and then corrected from the basis set superposition error (BSSE) by incorporating the counterpoise (CP) correction procedure.[71] Subsequently, the obtained energetic values were benchmarked at the CCSD/CBS level of theory, as given in the following eqns:[72,73]

$$E_{CCSD(T)/CBS} = \Delta E_{MP2/CBS} + \Delta E_{CCSD(T)} \quad (2)$$

where:

$$\Delta E_{MP2/CBS} = (64E_{MP2/aug\text{-}cc\text{-}pVQZ(PP)} - 27E_{MP2/aug\text{-}cc\text{-}pVTZ(PP)})/37 \quad (3)$$

$$\Delta E_{CCSD(T)} = E_{CCSD(T)/aug\text{-}cc\text{-}pVdZ(PP)} - E_{MP2/aug\text{-}cc\text{-}pVDZ(PP)} \quad (4)$$

SAPT analysis[74] was performed using the PSI4 code[75] to unveil the force beyond the occurrence of the investigated interactions within the complexes understudy. The total SAPT2+(3)dMP2 interaction energy (E_{SAPT}) was computed by summing its main four physical components, namely dispersion (E_{disp}), exchange (E_{exch}), induction (E_{ind}), and electrostatic (E_{elst}), as illustrated in eqn (5)–(9).[76]

$$E_{SAPT} = E_{elst} + E_{exch} + E_{ind} + E_{disp} \quad (5)$$

where:

$$E_{elst} = E_{elst}^{(10)} + E_{elst}^{(12)} + E_{elst}^{(13)} \quad (6)$$

$$E_{exch} = E_{exch}^{(10)} + E_{exch}^{(11)} + E_{exch}^{(12)} \quad (7)$$

$$E_{ind} = E_{ind,resp}^{(20)} + E_{exch\text{-}ind,resp}^{(20)} + E_{ind,resp}^{(22)} + E_{exch\text{-}ind,resp}^{(22)} + \delta E_{HF}^{(2)} + \delta E_{MP2}^{(2)} \quad (8)$$

$$E_{disp} = E_{disp}^{(20)} + E_{exch\text{-}disp}^{(20)} + E_{disp}^{(21)} + E_{disp}^{(22)}(SDQ) + E_{disp}^{(22)}T + E_{disp}^{(30)} \quad (9)$$

In an attempt to provide a comprehensive understanding of the bonding features of the complexes understudy, QTAIM[77] and NCI index techniques were applied.[58] Further understanding of the EEF influence on the σ-, lp-, and π-hole site-based interactions was established by employing EEF along the *z*-axis with variant strength in the range of 0.004–0.016 au. For the optimized aerogen-comprising molecules, the structures were reoptimized in the presence of ±0.004, ±0.008, and ±0.016 au EEF. ESP analysis was carried out on the obtained structures under the same EEF conditions. For the complexes under study, geometrical optimization and interaction energy computations were also performed using EEF of +0.004, +0.008, and +0.016 au. The computations of the ESP, PoC, QTAIM and NCI analyses were accomplished employing the Gaussian 09 software[78] at the MP2/aug-cc-pVTZ(PP) level of theory. Multiwfn 3.7 software[68] was utilized to execute the QTAIM and NCI calculations. Plots of QTAIM and NCI were conceived with the assistance of the Visual Molecular Dynamics program.[79]

4. Conclusions

In the current research, the ability of ZO_3 and ZF_2 aerogen-comprising molecules to form σ-/lp- and π-hole, respectively, with NH_3 and NCH Lewis bases was comparatively investigated. Sundry *ab initio* computations involving ESP, PoC, interaction energy, QTAIM, NCI, and SAPT were performed. A premier understanding of the EEF influence on the complexation and energetic features of the σ-, lp-, and π-hole site-based interactions was obtained utilizing the oriented EEF with disparate magnitudes. The ESP outcomes confirmed the existence of positive σ-/lp- and π-hole over the ZO_3 and ZF_2 molecular structures, respectively, with observable appearance for σ-hole. The computed interaction energy quantities announced σ-hole site-based interactions with higher preferability than the other ones. Interestingly, the strength of the σ- and lp-hole site-based interactions directly correlated with the aerogen atomic size and the magnitude of the positively oriented EEF. In comparison, the strength of the π-hole site-based interaction showed an irregular correlation with the aerogen atomic size. Nevertheless, by applying the positively oriented EEF with high strength, a direct proportion between the strength of the latter interactions and aerogen atomic size was obtained. The emerging outcomes would be beneficial for forthcoming studies pertinent to the characterization of the σ-, lp-, and π-hole site-based interactions within aerogen-comprising complexes and their analogical applications.

Data availability

The data supporting this article have been included as part of the ESI.†

Author contributions

Conceptualization, Mahmoud A. A. Ibrahim and Tamer Shoeib; methodology, Mahmoud A. A. Ibrahim, Nayra A. M. Moussa, and Mohamed Khaled Abd El-Rahman; software, Mahmoud A. A. Ibrahim; formal analysis, Hassan A. A. Abuelliel; investigation, Hassan A. A. Abuelliel and Nayra A. M. Moussa; resources, Mahmoud A. A. Ibrahim, Shaban R. M. Sayed, Mohamed A. El-Tayeb and Tamer Shoeib; data curation, Hassan A. A. Abuelliel; writing—original draft preparation, Hassan A. A. Abuelliel and Alshimaa S. M. Rady; writing—review and editing, Mahmoud A. A. Ibrahim, Nayra A. M. Moussa, Mohamed A. El-Tayeb, Shaban R. M. Sayed, Muhammad Naeem Ahmed, Mohamed Khaled Abd El-Rahman, and Tamer Shoeib; visualization, Hassan A. A. Abuelliel and Muhammad Naeem Ahmed; supervision, Mahmoud A. A. Ibrahim; project administration, Mahmoud A. A. Ibrahim, Nayra A. M. Moussa and Tamer Shoeib. All authors have read and agreed to the published version of the manuscript.

Conflicts of interest

There are no conflicts to declare.

Acknowledgements

The authors extend their appreciation to the Researchers Supporting Project number (RSPD2024R678), King Saud University, Riyadh, Saudi Arabia, for funding this work. The computational work was completed with resources provided by the CompChem Lab (Minia University, Egypt, http://hpc.compchem.net), Center for High-Performance Computing (Cape Town, South Africa, http://www.chpc.ac.za), Bibliotheca Alexandrina (http://hpc.bibalex.org), and the American University in Cairo.

References

1 I. Alkorta, J. Elguero and A. Frontera, *Crystals*, 2020, **10**, 180–208.
2 P. R. Varadwaj, A. Varadwaj, H. M. Marques and K. Yamashita, *Sci. Rep.*, 2019, **9**, 50.
3 K. E. Riley and P. Hobza, *Wiley Interdiscip. Rev.: Comput. Mol. Sci.*, 2011, **1**, 3–17.
4 E. Frieden, *J. Chem. Educ.*, 1975, **52**, 754–756.
5 X. de la Cruz, J. Reverter and I. Fita, *J. Mol. Graphics*, 1992, **10**, 96–100.
6 D. Braga and F. Grepioni, *Acc. Chem. Res.*, 2000, **33**, 601–608.
7 J. M. A. Robinson, D. Philp, K. D. M. Harris and B. M. Kariuki, *New J. Chem.*, 2000, **24**, 799–806.
8 J. Y. C. Lim and P. D. Beer, *Chem*, 2018, **4**, 731–783.
9 D. Mani and E. Arunan, *J. Phys. Chem. A*, 2014, **118**, 10081–10089.
10 G. Mahmoudi, A. Bauza, M. Amini, E. Molins, J. T. Mague and A. Frontera, *Dalton Trans.*, 2016, **45**, 10708–10716.
11 W. J. Vickaryous, R. Herges and D. W. Johnson, *Angew. Chem., Int. Ed.*, 2004, **43**, 5831–5833.
12 K. Muller-Dethlefs and P. Hobza, *Chem. Rev.*, 2000, **100**, 143–168.
13 L. P. Wolters, P. Schyman, M. J. Pavan, W. L. Jorgensen, F. M. Bickelhaupt and S. Kozuch, *Wiley Interdiscip. Rev.: Comput. Mol. Sci.*, 2014, **4**, 523–540.
14 Y. Lu, Y. Wang and W. Zhu, *Phys. Chem. Chem. Phys.*, 2010, **12**, 4543–4551.
15 Y. Lu, Y. Liu, Z. Xu, H. Li, H. Liu and W. Zhu, *Expert Opin. Drug Discovery*, 2012, **7**, 375–383.
16 D. A. Uhlenheuer, K. Petkau and L. Brunsveld, *Chem. Soc. Rev.*, 2010, **39**, 2817–2826.
17 D. K. Smith, *J. Chem. Educ.*, 2005, **82**, 393–400.
18 A. Bauza, T. J. Mooibroek and A. Frontera, *Chem. Commun.*, 2014, **50**, 12626–12629.
19 T. Clark, M. Hennemann, J. S. Murray and P. Politzer, *J. Mol. Model.*, 2007, **13**, 291–296.
20 J. S. Murray, P. Lane, T. Clark, K. E. Riley and P. Politzer, *J. Mol. Model.*, 2012, **18**, 541–548.
21 M. A. A. Ibrahim, R. R. A. Saeed, M. N. I. Shehata, N. A. M. Moussa, A. M. Tawfeek, M. N. Ahmed, M. K. Abd El-Rahman and T. Shoeib, *ACS Omega*, 2023, **8**, 32828–32837.
22 M. A. A. Ibrahim, Y. A. M. Mohamed, H. S. M. Abd Elhafez, M. N. I. Shehata, M. E. S. Soliman, M. N. Ahmed, H. R. Abd El-Mageed and N. A. M. Moussa, *J. Mol. Graphics Modell.*, 2022, **111**, 108097.
23 S. J. Grabowski, *ChemPhysChem*, 2014, **15**, 2985–2993.
24 S. J. Grabowski, *Molecules*, 2015, **20**, 11297–11316.
25 L. Gao, Y. Zeng, X. Zhang and L. Meng, *J. Comput. Chem.*, 2016, **37**, 1321–1327.
26 A. Bauza, T. J. Mooibroek and A. Frontera, *Angew. Chem., Int. Ed.*, 2013, **52**, 12317–12321.
27 W. Zierkiewicz, M. Michalczyk and S. Scheiner, *Molecules*, 2018, **23**, 1416.
28 A. Grabarz, M. Michalczyk, W. Zierkiewicz and S. Scheiner, *ChemPhysChem*, 2020, **21**, 1934–1944.
29 M. Hou, Z. Liu and Q. Li, *Int. J. Quantum Chem.*, 2020, **120**, e26251.
30 I. Alkorta, J. Elguero and J. E. Del Bene, *J. Phys. Chem. A*, 2013, **117**, 10497–10503.
31 S. Scheiner, *Acc. Chem. Res.*, 2013, **46**, 280–288.
32 A. Bauza, R. Ramis and A. Frontera, *J. Phys. Chem. A*, 2014, **118**, 2827–2834.
33 A. Bauza, T. J. Mooibroek and A. Frontera, *ChemPhysChem*, 2016, **17**, 1608–1614.
34 M. D. Esrafili and R. Nurazar, *Mol. Phys.*, 2015, **114**, 276–282.
35 C. B. Aakeroy, D. L. Bryce, G. Desiraju, A. Frontera, A. C. Legon, F. Nicotra, K. Rissanen, S. Scheiner, G. Terraneo, P. Metrangolo and G. Resnati, *Pure Appl. Chem.*, 2019, **91**, 1889–1892.
36 P. Politzer, J. S. Murray and T. Clark, *Phys. Chem. Chem. Phys.*, 2010, **12**, 7748–7757.
37 M. A. A. Ibrahim and A. A. M. Hasb, *Theor. Chem. Acc.*, 2019, **138**, 2–13.

38 H. Wang, W. Wang and W. J. Jin, *Chem. Rev.*, 2016, **116**, 5072–5104.
39 A. Bauza and A. Frontera, *Angew. Chem.*, 2015, **54**, 7340–7343.
40 A. Bauza and A. Frontera, *Phys. Chem. Chem. Phys.*, 2015, **17**, 24748–24753.
41 M. D. Esrafili, S. Asadollahi and M. Vakili, *Int. J. Quantum Chem.*, 2016, **116**, 1254–1260.
42 R. M. Gomila and A. Frontera, *Front. Chem.*, 2020, **8**, 395.
43 F. M. Carvalho, A. S. Kiametis, A. L. de Araujo Oliveira, F. Pirani and R. Gargano, *Spectrochim. Acta, Part A*, 2021, **246**, 119049.
44 M. D. Esrafili, F. Mohammadian-Sabet and M. Solimannejad, *Chem. Phys. Lett.*, 2016, **659**, 196–202.
45 M. D. Esrafili and E. Vessally, *Chem. Phys. Lett.*, 2016, **662**, 80–85.
46 W. Zierkiewicz, M. Michalczyk and S. Scheiner, *Phys. Chem. Chem. Phys.*, 2018, **20**, 4676–4687.
47 J. Miao, Z. Xiong and Y. Gao, *J. Phys.: Condens.Matter*, 2018, **30**, 444001.
48 T. Lang, X. Li, L. Meng, S. Zheng and Y. Zeng, *Struct. Chem.*, 2014, **26**, 213–221.
49 M. Solimannejad, N. Nassirinia and S. Amani, *Struct. Chem.*, 2012, **24**, 651–659.
50 M. Solimannejad, V. Ramezani, C. Trujillo, I. Alkorta, G. Sanchez-Sanz and J. Elguero, *J. Phys. Chem. A*, 2012, **116**, 5199–5206.
51 S. A. C. McDowell and J. A. Joseph, *Mol. Phys.*, 2014, **113**, 16–21.
52 A. Bauza and A. Frontera, *ChemPhysChem*, 2016, **17**, 3181–3186.
53 M. E. Alikhani, *J. Mol. Model.*, 2020, **26**, 94.
54 Y. Deng, Zanzhang, W. Cao, Y. Liu, B. Zheng and Z. Wang, *J. Mol. Model.*, 2022, **28**, 339.
55 M. A. A. Ibrahim, S. M. A. Saad, J. H. Al-Fahemi, G. A. H. Mekhemer, S. A. Ahmed, A. M. Shawky and N. A. M. Moussa, *RSC Adv.*, 2021, **11**, 4022–4034.
56 M. Kolar, J. Hostas and P. Hobza, *Phys. Chem. Chem. Phys.*, 2014, **16**, 9987–9996.
57 M. A. A. Ibrahim, M. N. I. Shehata, M. E. S. Soliman, M. F. Moustafa, H. R. A. El-Mageed and N. A. M. Moussa, *Phys. Chem. Chem. Phys.*, 2022, **24**, 3386–3399.
58 E. R. Johnson, S. Keinan, P. Mori-Sanchez, J. Contreras-Garcia, A. J. Cohen and W. Yang, *J. Am. Chem. Soc.*, 2010, **132**, 6498–6506.
59 J. Contreras-Garcia, E. R. Johnson, S. Keinan, R. Chaudret, J. P. Piquemal, D. N. Beratan and W. Yang, *J. Chem. Theory Comput.*, 2011, **7**, 625–632.
60 B. J. Dutta and P. K. Bhattacharyya, *Int. J. Quantum Chem.*, 2015, **115**, 1459–1466.
61 M. A. A. Ibrahim, N. A. M. Moussa, A. A. K. Kamel, M. N. I. Shehata, M. N. Ahmed, F. Taha, M. A. S. Abourehab, A. M. Shawky, E. B. Elkaeed and M. E. S. Soliman, *Molecules*, 2022, **27**, 2963.
62 M. A. A. Ibrahim, N. A. M. Moussa, S. M. A. Saad, M. N. Ahmed, A. M. Shawky, M. E. S. Soliman, G. A. H. Mekhemer and A. S. M. Rady, *ACS Omega*, 2022, **7**, 11264–11275.
63 C. Møller and M. S. Plesset, *Phys. Rev.*, 1934, **46**, 618–622.
64 D. E. Woon and T. H. Dunning, *J. Chem. Phys.*, 1993, **98**, 1358–1371.
65 D. E. Woon and T. H. Dunning, *J. Chem. Phys.*, 1994, **100**, 2975–2988.
66 D. Feller, *J. Comput. Chem.*, 1996, **17**, 1571–1586.
67 M. A. A. Ibrahim, *J. Mol. Model.*, 2012, **18**, 4625–4638.
68 T. Lu and F. Chen, *J. Comput. Chem.*, 2012, **33**, 580–592.
69 M. A. A. Ibrahim, R. R. A. Saeed, M. N. I. Shehata, M. N. Ahmed, A. M. Shawky, M. M. Khowdiary, E. B. Elkaeed, M. E. S. Soliman and N. A. M. Moussa, *Int. J. Mol. Sci.*, 2022, **23**, 3114.
70 M. A. A. Ibrahim, R. R. A. Saeed, M. N. I. Shehata, E. E. B. Mohamed, M. E. S. Soliman, J. H. Al-Fahemi, H. R. A. El-Mageed, M. N. Ahmed, A. M. Shawky and N. A. M. Moussa, *J. Mol. Struct.*, 2022, **1265**, 133232.
71 S. F. Boys and F. Bernardi, *Mol. Phys.*, 1970, **19**, 553–566.
72 B. K. Mishra, S. Karthikeyan and V. Ramanathan, *J. Chem. Theory Comput.*, 2012, **8**, 1935–1942.
73 T. Helgaker, W. Klopper, H. Koch and J. Noga, *J. Chem. Phys.*, 1997, **106**, 9639–9646.
74 E. G. Hohenstein and C. D. Sherrill, *J. Chem. Phys.*, 2010, **132**, 184111–184120.
75 J. M. Turney, A. C. Simmonett, R. M. Parrish, E. G. Hohenstein, F. A. Evangelista, J. T. Fermann, B. J. Mintz, L. A. Burns, J. J. Wilke, M. L. Abrams, N. J. Russ, M. L. Leininger, C. L. Janssen, E. T. Seidl, W. D. Allen, H. F. Schaefer, R. A. King, E. F. Valeev, C. D. Sherrill and T. D. Crawford, *Wiley Interdiscip. Rev.: Comput. Mol. Sci.*, 2012, **2**, 556–565.
76 T. M. Parker, L. A. Burns, R. M. Parrish, A. G. Ryno and C. D. Sherrill, *J. Chem. Phys.*, 2014, **140**, 094106.
77 R. F. W. Bader, *Acc. Chem. Res.*, 1985, **18**, 9–15.
78 M. J. Frisch, G. W. Trucks, H. B. Schlegel, G. E. Scuseria, M. A. Robb, J. R. Cheeseman, G. Scalmani, V. Barone, B. Mennucci, G. A. Petersson, H. Nakatsuji, M. Caricato, X. Li, H. P. Hratchian, A. F. Izmaylov, J. Bloino, G. Zheng, J. L. Sonnenberg, M. Hada, M. Ehara, K. Toyota, R. Fukuda, J. Hasegawa, M. Ishida, T. Nakajima, Y. Honda, O. Kitao, H. Nakai, T. Vreven, J. A. Montgomery, J. E. Peralta, F. Ogliaro, M. Bearpark, J. J. Heyd, E. Brothers, K. N. Kudin, V. N. Staroverov, R. Kobayashi, J. Normand, K. Raghavachari, A. Rendell, J. C. Burant, S. S. Iyengar, J. Tomasi, M. Cossi, N. Rega, J. M. Millam, M. Klene, J. E. Knox, J. B. Cross, V. Bakken, C. Adamo, J. Jaramillo, R. Gomperts, R. E. Stratmann, O. Yazyev, A. J. Austin, R. Cammi, C. Pomelli, J. W. Ochterski, R. L. Martin, K. Morokuma, V. G. Zakrzewski, G. A. Voth, P. Salvador, J. J. Dannenberg, S. Dapprich, A. D. Daniels, Ö. Farkas, J. B. Foresman, J. V. Ortiz, J. Cioslowski and D. J. Fox, *Gaussian 09 Revision E01, Gaussian09*, Gaussian Inc., Wallingford CT, USA.
79 W. Humphrey, A. Dalke and K. Schulten, *J. Mol. Graphics*, 1996, **14**, 33–38.